OPTIMIZATION OF CHABOCHE KINEMATIC HARDENING PARAMETERS BY
USING AN ALGEBRAIC METHOD BASED ON INTEGRAL EQUATIONS

Liu Shijie and Liang Guozhu

msp

msp

OPTIMIZATION OF CHABOCHE KINEMATIC HARDENING PARAMETERS BY USING AN ALGEBRAIC METHOD BASED ON INTEGRAL EQUATIONS

LIU SHIJIE AND LIANG GUOZHU

The current work is devoted to optimizing the Chaboche kinematic hardening parameters via an algebraic method based on its integral equations, which is rarely investigated. An experimental test in strain range of ±0.8% for 304 stainless steel (304SS) is applied to demonstrate this method. Firstly, the first quarter tensile part, along with the Osgood–Ramberg equation, is used to estimate the initial parameters. Then, optimizations are conducted based on the first quarter tensile part for the first and the 150th cyclic test. Results indicate that:

  (i) the value of initial yielding stress has a significant effect on the simulation. The optimized initial yielding stress is roughly 181 MPa for 304SS, which corresponds to the test at strain range of ±0.8% with a frequency of 0.25 Hz.
 (ii) The experimental plastic strains in elastic loading/unloading segments in the proposed method are unreasonable in calculating the stresses and should be removed before conducting an optimization.

A list of symbols can be found on page 453.

1. Introduction

It is well-known that metallic materials exhibit a gradual fatigue life consumption phenomenon under a complicated cyclic loading. Indeed, the cyclic deformation, including ratcheting, of metallic structures has been extensively studied in the last few decades, as it plays a very important role in safety assessments and fatigue-life estimations.

Many experimental studies were conducted about mechanical behaviors subjected to cyclic loading [Prager 1956; Benham 1965; Kamaya and Kawakubo 2015]. Along with those experimental studies, many researchers have tried to develop appropriate constitutive models to better predict the response of metallic materials subjected to cyclic loading, especially the Bauchinger effect and the strain accumulation in unsymmetric uniaxial stress-controlled conditions. The first systematic literature in this regard is [Prager 1956], in which the author proposed a linear hardening model capable of capturing the Bauchinger effect; however, the model failed to simulate ratcheting strains in the presence of mean stress due to its constant plastic hardening modulus. For this reason, in [Armstrong and Frederick 1966], the authors modified Prager's hardening rule by adding a nonlinear recall term to propose the so-called Armstrong and Frederick hardening model. This new term could account for the fading memory effect of the plastic strain path observed in experiments by making a difference in the plastic hardening modulus between the forward and reverse parts in a typical unsymmetric stress cycle. Due to this initial work of Armstrong and Frederick, the idea of describing the evolution of kinematic hardening variables in terms of nonlinear differential equations has been followed in many other studies, such as [Chaboche

et al. 1979; Chaboche 1991; 2008]. The Chaboche model is a decomposed nonlinear kinematic hardening model (CHK-M, where M is the total number of AF rules in the Chaboche kinematic hardening model), in which each of the backstress components plays a primary role in controlling the shape of σ-ε response at different ranges of strain. The CHK-M model is rate-independent and able to account for the Bauschinger effect. The advantage of this model is that it can be modified to solve for complex behaviors of the materials under various conditions. Besides the CHK-M model, many other evolution of kinematic hardening models have been proposed; see, e.g., [Ohno and Wang 1994; Voyiadjis and Basuroychowdhury 1998; Bari and Hassan 2000; Dafalias et al. 2008; Abdel-Karim 2010; Ahmadzadeh and Varvani-Farahani 2013; Jiang et al. 2013]. Note that the multimechanism model has attracted attention in the last twenty years. In [Velay et al. 2006], the authors proposed a nonunified elasto-plastic model for describing the TMF behavior of AISI L6. Two integration methods, explicit Runge–Kutta method and implicit θ method, of constitutive equations were developed for the numerical implementation of the 2-mechanisms -1 yield criterion (2M1C) model. Based on the modification of 2M1C model, a new version of the multimechanism model for plasticity was proposed in [Taleb and Cailletaud 2010] for considering the nonproportional effect of the loading and the strain memory phenomenon. In the previous work, the kinematic hardening parameters were identified by using optimization software included in the finite element method (FEM) code ZeBuLoN. The optimization algorithms in the software are shown in [Besson et al. 1998].

Among various constitutive models mentioned above, the CHK-M model was widely used [Abdel-Karim 2010; Jiang et al. 2009; Djimli et al. 2010]. As suggested in [Chaboche et al. 1979; Chaboche 1986], at least three AF rules should be incorporated in the model. Because of its simplicity and efficiency, this model was implemented into different kinds of finite element software (e.g., ABAQUS and ANSYS).

The CHK-M model has been applied for decades and the metal-related fatigue literature are numerous, for example, [Egner and Egner 2014; Pereira and Jesus 2011; Chaboche 1988; Jiang et al. 2009]. Indeed, higher accuracy of the predicted material cyclic mechanical behavior accompanies higher accuracy of fatigue life estimation. Consequently, in order to get an accurate description of fatigue material behavior and its properties [Chaboche et al. 2012; Djimli et al. 2010; Li et al. 2014], it is necessary to choose or develop a suitable constitutive model that will accurately describe its mechanical behavior of materials. While the identification of material parameters in various hardening models is always one of the principal difficulties to be handled prior to the fatigue life estimation, the parameters of CHK-M model can be identified by using the finite element method with the return-mapping algorithm through a trial-and-error approach. However, this method is difficult to implement, especially for practical applications, because the test data are mainly being used to validate the parameters, not to identify them (which is rather time consuming). In this case, an algebraic approach simulating the stress with the integral equations was developed to predict and optimize the CHK-M model parameters, which directly identifies the model parameters based on the test data. The current work is to determine the CHK-M model parameters in the cyclic experimental tests under strain-controlled conditions, but isotropic hardening/softening and ratcheting are not taken into account.

2. Optimization method of model parameters identification

There exist a lot of yield criteria for determining the yield condition, among which the von Mises criterion is widely used. The yield surface, regarding the plasticity criterion, of a purely kinematic hardening von

Mises material can be written as

$$f(\underset{\approx}{\sigma}, \underset{\approx}{X}) = \sqrt{\tfrac{3}{2}(\underset{\approx}{s} - \underset{\approx}{X}) : (\underset{\approx}{s} - \underset{\approx}{X})} - k = 0, \tag{1}$$

where the backstress tensor $\underset{\approx}{X}$ defines the current center of the yield surface in the stress space.

Actually, the Chaboche decomposed hardening model [Chaboche et al. 1979; Chaboche 1986] is an assembly of several AF rules, which can be expressed as

$$d\underset{\approx}{X} = \sum_{i=1}^{M} d\underset{\approx}{X}_i, \quad d\underset{\approx}{X}_i = \tfrac{2}{3}C_i d\underset{\approx}{\varepsilon}_p - \gamma_i \underset{\approx}{X}_i dp, \quad dp = \sqrt{\tfrac{2}{3}d\underset{\approx}{\varepsilon}_p : d\underset{\approx}{\varepsilon}_p}, \tag{2}$$

where M is the total number of decomposed AF rules utilized. The main reason for the superposition of several AF rules in the Chaboche model is to improve its accuracy at different ranges of strain; as stated in Section 1, the goal cannot be achieved using only one AF rule. Chaboche [1986] first used the superposition of three AF rules ($M = 3$) to simulate the three critical segments of monotonic stress-strain curves and this method is also adopted in the current study.

In the case of uniaxial loading, each of the decomposed rules takes the form

$$dX_x = \sum_{i=1}^{M} dX_{ix}, \quad dX_{ix} = \tfrac{2}{3}C_i d\varepsilon_{p,x} - \gamma_i X_{ix}|d\varepsilon_{p,x}|, \tag{3}$$

where the subscript x stands for the direction of applied load. Now, it can be easily shown that the following equation holds between the uniaxial stress, the backstress, and the initial yielding stress:

$$\left| \sigma_x - \tfrac{3}{2}X_x \right| = k. \tag{4}$$

For simplicity, the subscript x was omitted for deducing the integral equation for (3) in uniaxial state. Furthermore, combining (3) and (4), the decomposed component equation in (3) will be $dX_i = C_i d\varepsilon_p - \gamma_i X_i |d\varepsilon_p|$.

In the first quarter tensile part, $v = \operatorname{sign} \dot{\varepsilon}_p = 1$ and starts from the initial virgin state ($\varepsilon_{p,0} = 0$, $X_{i,0} = 0$). Integrating (3), we have

$$X_{i,j} = \frac{C_i}{\gamma_i}[1 - \exp(\gamma_i \varepsilon_{p,j})] \quad (i = 1, 2, \ldots, M), \tag{5}$$

where the subscript j denotes the serial number of plastic strain used. In (5), for $\varepsilon_{p,j} \to \infty$, the stress asymptotically approaches a limit value C_i/γ_i. This means that the kinematic hardening process becomes saturated and the backstress cannot exceed $X_{i,\infty} = C_i/\gamma_i$.

If the loading direction is reversed at plastic strain ε_{p,N_1} and the corresponding backstress at ε_{p,N_1} is $X_{i,N_1} = X_{i,\infty}[1 - \exp(-\gamma_i \varepsilon_{p,N_1})]$, the subsequent evolution of backstress is given by

$$\begin{aligned} X_{i,j} &= -\frac{C_i}{\gamma_i} + \left(X_{i,N_1} + \frac{C_i}{\gamma_1}\right)\exp[\gamma_1(\varepsilon_{p,j} - \varepsilon_{p,N_1})] \\ &= -X_{i,\infty} + (X_{i,N_1} + X_{i,\infty})\exp[\gamma_i(\varepsilon_{p,j} - \varepsilon_{p,N_1})]. \end{aligned} \tag{6}$$

Similarly denoting X_{i,N_2} and ε_{p,N_2} as the final values of $X_{i,j}$ and $\varepsilon_{p,j}$ for (6), the backstress at ε_{p,N_2} is

$$X_{i,N_2} = -X_{i,\infty} + (X_{i,N_1} + X_{i,\infty})\exp[\gamma_i(\varepsilon_{p,N_2} - \varepsilon_{p,N_1})].$$

The evolution of the backstress from compression to tension is given as

$$
\begin{aligned}
X_{i,j} &= \frac{C_i}{\gamma_i} + \left(X_{i,N_2} - \frac{C_i}{\gamma_i} \right) \exp[-\gamma_i(\varepsilon_{p,j} - \varepsilon_{p,N_2})] \\
&= X_{i,\infty} + (X_{i,N_2} - X_{i,\infty}) \exp[-\gamma_i(\varepsilon_{p,j} - \varepsilon_{p,N_2})].
\end{aligned}
\tag{7}
$$

By means of (7), the backstress from the compressive tip ε_{p,N_2} to the tensile endpoint ε_{p,N_3} can be calculated. Then, the backstress-strain response is determined with equations (5)–(7). Substituting the total backstress $X_j = \sum_{i=1}^{M} X_{i,j}$ into (4), the total simulated stress σ_j^{sim} can be identified. Thus, the simulated stresses can all be calculated with equations (4)–(7). It is convenient to obtain the backstress-strain curve because only algebraic calculations exist in the above-mentioned method.

It is difficult identifying a set of reasonable CHK-M model parameters when using the traditional trial-and-error method. The well-known L-M nonlinear least square algorithm is a good tool in determining optimal model parameters, especially for the nonlinear system employed in the current work.

In the optimization, the differences between the stress values from the numerical simulated stress σ_j^{sim} and experimental measured stress σ_j^{exp} are represented in the following objective function F:

$$
F = \tfrac{1}{2} \sum_{j=1}^{N} (\sigma_j^{\text{sim}} - \sigma_j^{\text{exp}})^2,
$$

where N is the total number of the data points used in the optimization. The optimum values can be determined when the objective function reaches the specified convergence criterion, which is set to $1 \cdot 10^{-6}$ in the current work. Referring to the rules suggested in [Bari and Hassan 2000], parameters C_1, C_2, and C_3 are all constrained within the range of 100 to $1 \cdot 10^8$. In addition, γ_1 and γ_2 are in the range of 1 to $1 \cdot 10^4$, and then the constraint interval for γ_3 is [0.1, 6].

3. Study procedures

For the material 304SS, three groups of strain-controlled fatigue tests were performed at the material level, and the fatigue test at 0.8% strain amplitude was employed so as to identify the CHK-3 model parameters. Figure 1 is the detailed flow chart of the study procedures.

In Figure 1, the Ramberg–Osgood equation is applied to approximately represent the first quarter tensile part by using the L-M algorithm. After determining the parameters in the Ramberg–Osgood equation, the Chaboche kinematic hardening parameter C_i can be obtained by taking the derivative of the Ramberg–Osgood equation with plastic strain. Subsequently, the other relevant parameters γ_i can be predicted through allocating contribution percentages for every AF rule.

As indicated in [Dafalias et al. 2008], if the first quarter tensile segment includes a yield plateau that is significantly different from the hysteresis curve, then it is impossible to attempt to simulate all the curves by using one set of parameters. Conveniently, the first quarter tensile segment is used for estimating the initial parameters because $p = \varepsilon_p$ in the region and further optimizations can be performed to obtain more reasonable ones. Note that a reasonable initial yielding stress is beneficial for the stress-strain simulation. So the initial yielding stress and the hardening parameters for the first quarter tensile part was optimized in the current work. In order to verify the feasibility of these parameters for cyclic tests, the stress-strain response for the first cycle was simulated. Poor accuracy causes further optimization of
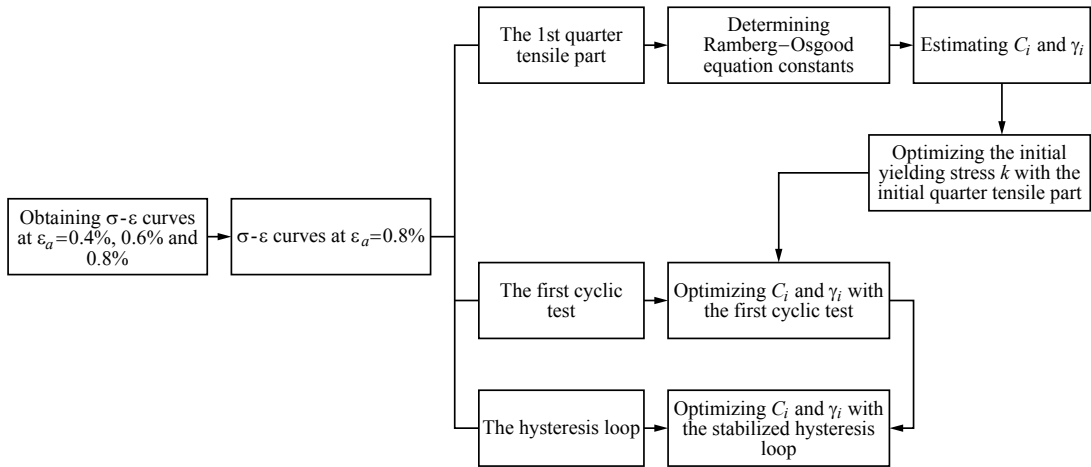
Figure 1. Study procedures of identifying CHK-3 model parameters.

parameters for the first cyclic test. Then, an investigation for the stabilized hysteresis loop was executed. As pointed out in previous literature [Bari and Hassan 2000; Ahmadzadeh and Varvani-Farahani 2013], the ratcheting parameter γ_3 in the third AF hardening rule should be constrained to a small range, such as [0.5, 10]. First, in order to verify the feasibility of the approach for the ratcheting simulation, the ratcheting parameter γ_3 was constrained within the interval from 0.1 to 6. Then, in order to improve the simulation accuracy for the stabilized hysteresis loop, the ratcheting parameter γ_3 was set to whatever the ratcheting strain is. Although the ratcheting issue was not included in the investigation, the ratcheting actually exists when using the parameters to perform a simulation.

4. Experimental testing

4.1. *Test specimen.* 304SS was chosen to verify the general method because it is cheap and it has extensive applications in industry. Table 1 shows the chemical composition of 304SS. In order to homogenize the 304SS material to obtain the expected mechanical properties, the steel ingots were forged into bars at 1160 °C. Then, an annealing treatment was performed by heating the bars up to 720 °C and cooling very slowly to room temperature. All experimental tests were conducted by using round-bar specimens. Figure 2 shows the test specimen.

4.2. *Test program.* Three groups of strain-controlled LCF tests were conducted, which were controlled by using the triangular waveform at a constant frequency of 0.25 Hz with a strain ratio $R_\varepsilon = -1$ and strain amplitude ε_a of 0.4%, 0.6%, and 0.8%. A 25 mm gauge extensometer was used for measuring and controlling the strain in the specimen and all tests were carried out according to the ASTM standard [ASTM

C	Si	Mn	P	S	C	Ni	Mo
≤ 0.08	≤ 1	≤ 2	≤ 0.045	≤ 0.03	> 17.03	> 8.01	> 0.02

Table 1. Chemical compositions of the 304 stainless steel (wt%).
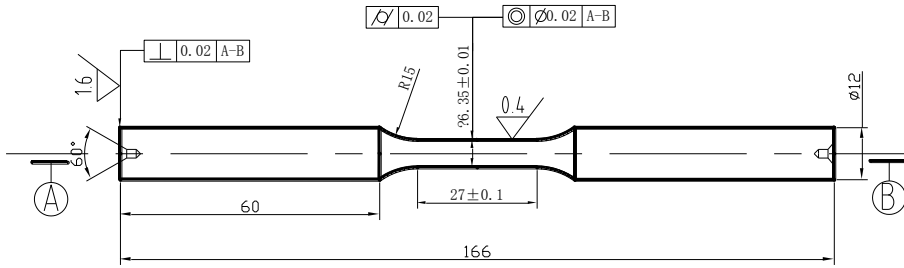
**Figure 2.** Specimen geometry used for strain-controlled fatigue test.

E606/E606M 2012]. The experiments were conducted on multiple specimens; namely, each test was carried out at a constant strain amplitude until failure occurred at room temperature.

4.3. *Experimental results.* First, we should determine which hysteresis loop could be suitably used for this study. Typical cyclic tests at different strain amplitudes are shown in Figure 3, left. It can be seen from Figure 3, left, that the reasonable strain range for identifying the CHK-3 model parameters is ±0.8%, which ensures that the first and the second AF rules get stabilized within the strain limit, while the third one does not. Therefore, the experimental test at a strain range of ±0.8% was used to obtain the CHK-3 model parameters.

The Chaboche kinematic hardening model is closely related to the plasticity. So, determining the plastic stress-strain response becomes a critical step in identifying its parameters.

Conveniently, the initial tensile curve (the first quarter cycle), OA, was used to estimate the parameters. Equation (3) is readily dealt with because of the relationship $p = \varepsilon_p$ in this segment.

The aforementioned first cyclic test at strain amplitude of 0.8%, together with its plastic stress-strain curve is displayed in Figure 3, right. As shown in this figure, the Young's modulus E is taken as the slope of the initial linear region. After performing a regression analysis for segment OP, the Young's modulus E is approximately 183500 MPa with the correlation efficient of 0.99887.
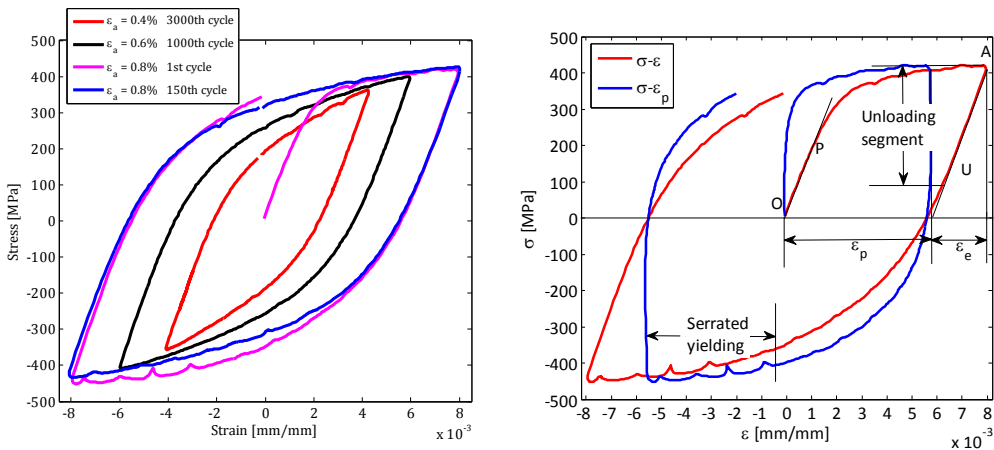
Figure 3. Left: LCF test results for 304 SS specimens. Right: The first cyclic test results at strain amplitude of 0.8%.

Some unreasonable problems exist, assuming all the plastic strain points are used to calculate the stress. The details are illustrated in the schematic diagram Figure 4. The Young's modulus E is the slope of the initial elastic loading segment OI. Theoretically, the plastic strain in OI is nearly equal to zero because of the relationship

$$\varepsilon_p = \varepsilon_T - \varepsilon_e = \varepsilon_T - \sigma/E = \varepsilon_T - \varepsilon_T = 0.$$

In addition, the test strain is portioned as

$$\varepsilon_T = \varepsilon_{th} + \varepsilon_{fl}.$$

In practice, the plastic strain in this region is not absolutely identical to zero due to the fluctuation. For example, the plastic strain in point B, ε_p^B, is negative because

$$\varepsilon_p^B = \varepsilon_T - \frac{\sigma_B}{E} = \varepsilon_T - \varepsilon_{th} = (\varepsilon_{th} + \varepsilon_{fl}) - \varepsilon_{th} = \varepsilon_{fl} < 0,$$

which leads to an unacceptable value when using (5) to simulate the backstress. This fact can be explained as follows:

$$X_{i,B} = \frac{C_i}{\gamma_i}[1 - \exp(\gamma_i \varepsilon_p^B)] < 0,$$

where $X_{i,B}$ is the backstress at point B. It is impossible that $X_{i,B}$ has a negative sign in the first quarter tensile part. Although the plastic strain in point A is positive, the simulated total stress at this point nearly equals the initial yielding stress, which will never approach the test stress. Therefore, points like A and B are called abnormal data in this investigation. In the elastic unloading part II-III, the ratio of ε_{fl} to ε_T is relatively small, which means the experimental plastic strain is very close to the theoretical. The theoretical plastic strain in II-III remains unchanged, as well-known. Thus, the simulated stress in II-III equals the stress at point II because such a small plastic strain fluctuation has little effect on
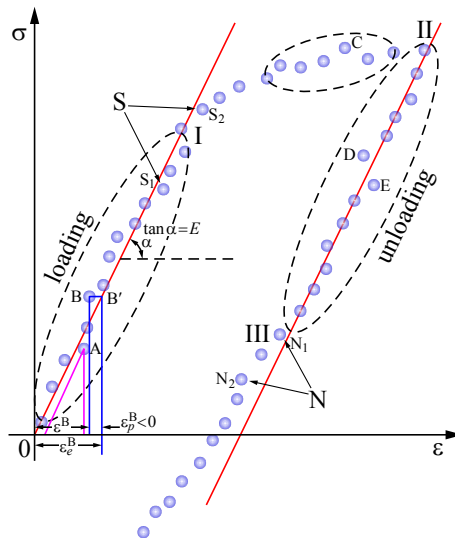
Figure 4. Schematic diagram of the cyclic stress-strain test response.
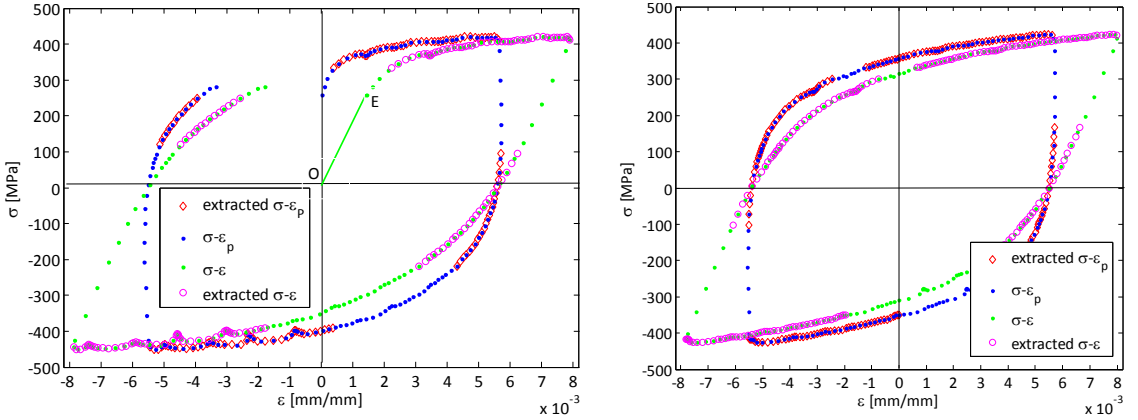
Figure 5. The effective first (left) and 150th (right) cyclic test data used for optimization.

the simulation. However, the experimental stress in II-III is gradually decreasing. In all, the simulated stresses in the elastic loading/unloading segments are not appropriate for use in the proposed method. Note that although the plastic strain fluctuation occurs in I-II, the calculated stress is acceptable. This fact can be partly explained by the analysis for II-III, and the simulated stress has a good tendency toward the experimental in this region.

Fortunately, the L-M algorithm is excellent for identifying the model parameters by using the subsequence extracted from the original test data. So, the elastic segments are removed in the following optimization.

Figure 5 shows the effective test data used for optimization, which are extracted from the original first and the 150th cyclic test curves.

5. Estimation of the initial values for the model parameters

As discussed in Section 2, the CHK-M model is a superposition of different AF rules; namely, the total back stress is the summation of backstress components. The AF hardening rule follows a series of successive specific slopes which are defined by the derivatives of backstress plastic strain curve, and the slope of the curve of AF rule gradually approaches zero with increasing plastic strain. Thus, a certain AF rule in the CHK-M model has a primary role in a special strain range, which means the other rules have a slight effect on the shape of the σ-ε curve in this range. For example, provided that the shape of σ-ε curve in strain range [0, 0.01%] is determined by the first AF rule, the influence by other AF rules can be ignored. Similarly, the second AF rule influences the shape of the σ-ε curve in the strain range [0.01%, 0.03%]. As a result, we can differentiate the first quarter tensile curve with respect to the plastic strain at different strain points to estimate the parameters C_i.

In order to efficiently and conveniently calculate parameters C_i, the Ramberg–Osgood equation is applied for approximating the first quarter tensile curve:

$$\frac{\varepsilon_T}{\varepsilon_0} = \frac{\sigma}{\sigma_0} + \left(\frac{\sigma}{\sigma_0}\right)^{n_0}. \tag{8}$$

The reason for using (8) to fit the first quarter tensile part is that the segment is similar to the mono-

tonic tensile curve. We use the following values for the Ramberg–Osgood constants of 304SS in the segment OA (strain amplitude of 0.8%):

$$n_0 = 5.3390, \quad \varepsilon_0 = 0.171\%, \quad \sigma_0 = 356\text{MPa}.$$

In order to verify the feasibility of these constants, the simulated stress-strain relationship was obtained by using the Ramberg–Osgood equation and shown in Figure 6 together with the first cyclic experimental test curve.

As shown in Figure 6, there exists a slight deviation between the simulation and the experimental test, particularly at the knee part. This may be ascribed to the quick hardening behavior of 304SS. However, the simulated curve has a good tendency for the real stress-strain curve, so the Ramberg–Osgood curve can be applied to predict the initial values of CHK-3 model parameters.

After obtaining the Ramberg–Osgood constants, the relationship of $\varepsilon_0 = \sigma_0/E$ can be substituted into (8) to give

$$\frac{E\varepsilon_T}{\sigma_0} = \frac{\sigma}{\sigma_0} + \left(\frac{\sigma}{\sigma_0}\right)^{n_0}, \tag{9}$$

which can then be differentiated with respect to ε_T to give

$$\frac{d\sigma}{d\varepsilon_T} = \frac{\sigma_0}{\varepsilon_0(1 + n_0(\sigma/\sigma_0)^{n_0-1})}. \tag{10}$$

The calculation of $d\sigma/d\varepsilon_p$ is more complicated. First, $d\sigma/d\varepsilon_p$ must be changed into the form

$$\frac{d\sigma}{d\varepsilon_p} = \frac{d\sigma}{d\varepsilon_T}\frac{d\varepsilon_T}{d\varepsilon_p} = \frac{d\sigma}{d\varepsilon_T}\frac{d\varepsilon_T/dt}{d\varepsilon_p/dt} = \frac{d\sigma}{d\varepsilon_T}\frac{1}{\dot{\varepsilon}_p}\dot{\varepsilon}_T. \tag{11}$$

Using Hooke's law and the total strain relationship, $d\varepsilon_p/dt$ can be given as

$$\frac{d\varepsilon_p}{dt} = \frac{d\varepsilon_T}{dt} - \frac{d\sigma}{dt}\frac{1}{E}. \tag{12}$$
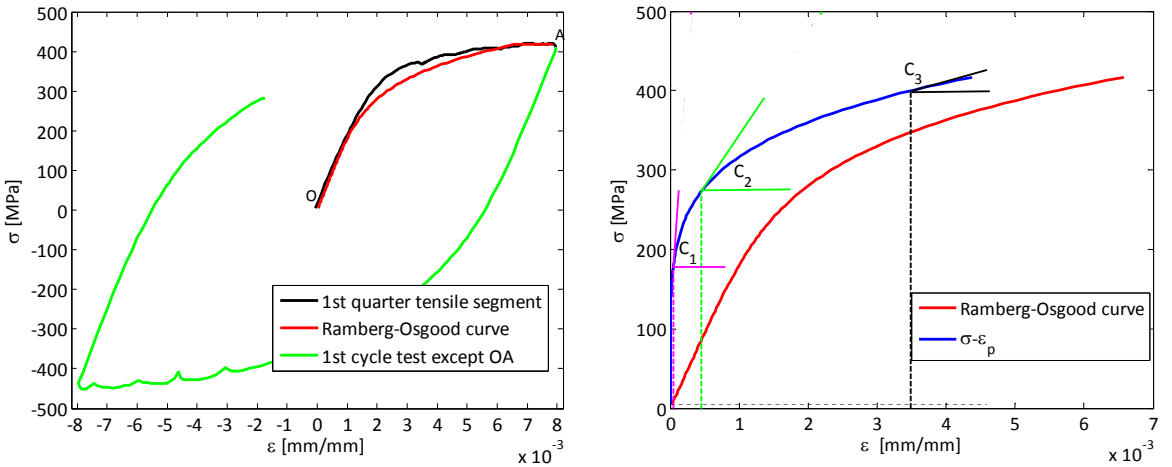
Figure 6. Left: comparison of the simulated Ramberg–Osgood curve and the first cyclic test curve. Right: The derivatives of the σ-ε_p curve at different points.

C_1	1249658.623	γ_1	42102.530
C_2	129813.037	γ_2	874.712
C_3	23817.112	γ_3	200.607

Table 2. Initial values of CHK-3 model parameters.

Then, (12) can be reformulated as

$$\frac{\mathrm{d}\varepsilon_p}{\mathrm{d}t} = \frac{\mathrm{d}\varepsilon_\mathrm{T}}{\mathrm{d}t} - \frac{\mathrm{d}\sigma}{\mathrm{d}t}\frac{1}{E}\frac{\mathrm{d}\varepsilon_\mathrm{T}}{\mathrm{d}\varepsilon_\mathrm{T}} = \frac{\mathrm{d}\varepsilon_\mathrm{T}}{\mathrm{d}t} - \frac{\mathrm{d}\sigma}{\mathrm{d}\varepsilon_\mathrm{T}}\frac{1}{E}\frac{\mathrm{d}\varepsilon_\mathrm{T}}{\mathrm{d}t} = \frac{\mathrm{d}\varepsilon_\mathrm{T}}{\mathrm{d}t}\left(1 - \frac{\mathrm{d}\sigma}{\mathrm{d}\varepsilon_\mathrm{T}}\frac{1}{E}\right). \tag{13}$$

So $\dot{\varepsilon}_p = \dot{\varepsilon}_\mathrm{T}\big(1 - (\mathrm{d}\sigma/\mathrm{d}\varepsilon_\mathrm{T})(1/E)\big)$, which means $\dot{\varepsilon}_\mathrm{T}/\dot{\varepsilon}_p = 1/\big(1 - (\mathrm{d}\sigma/\mathrm{d}\varepsilon_\mathrm{T})(1/E)\big)$.

The expression for $\mathrm{d}\sigma/\mathrm{d}\varepsilon_p$ can then be obtained expressed in terms of the derivative $\mathrm{d}\sigma/\mathrm{d}\varepsilon_\mathrm{T}$ by substituting $\dot{\varepsilon}_\mathrm{T}/\dot{\varepsilon}_p$ into (11):

$$\frac{\mathrm{d}\sigma}{\mathrm{d}\varepsilon_p} = \frac{\mathrm{d}\sigma}{\mathrm{d}\varepsilon_\mathrm{T}}\frac{1}{1 - (1/E)(\mathrm{d}\sigma/\mathrm{d}\varepsilon_\mathrm{T})}. \tag{14}$$

Since the Young's modulus has been confirmed, the plastic stress-strain response can be determined with the relationship $\varepsilon_p = \varepsilon_\mathrm{T} - \sigma/E$. Meanwhile, the slopes of the plastic stress-strain curve can also be given by (14). As a consequence, the tangent lines of the σ-ε_p curve can be identified, which are shown in Figure 6, right.

The AF rules contribution method, as described in [Rahman 2006], is applied for determining the parameters γ_i, which control the rate of the hardening modulus, which decreases with increasing plastic strain. In the tensile part, the total stress σ_x could be denoted by adding the summation of the backstresses of AF rules and the yield stress k, so the following relationship provides the reference for assigning the contribution fractions:

$$\frac{C_1}{\gamma_1} + \frac{C_2}{\gamma_2} + \left[\frac{C_3}{\gamma_3}\right] = \sigma_x - k. \tag{15}$$

Equation (15) indicates that the first and the second AF rule reach the saturated values before the testing strain attains its peak, while the third AF rule (embraced in a bracket) denotes that this component may not be up to its saturation value. The advantage of this strategy is that the first and the second AF rule respectively determine the shape of the initial and the knee part for the stress-strain curve; the third unsaturated AF rule controls the end part of the curve and the ratcheting strain evolution. Obviously, the right side of (15) can be readily determined. As a result, if the backstress contributions from each of the three AF rules in the left side of (15) can be determined, then the initial values of γ_1, γ_2, and γ_3 can be estimated. Following the data applied in [Rahman 2006], contribution fractions of 0.1, 0.5, and 0.3 are also applied for each of the three AF rules, respectively, in the current study.

Table 2 shows the initial values of CHK-3 model parameters estimated for the first quarter tensile part.

As illustrated above, the CHK-3 model parameters have been estimated successfully for the first quarter tensile segment, but in general, these parameters have poor accuracy for simulating the stabilized hysteresis loop, especially when the first quarter tensile segment includes a yield plateau. As depicted in Figure 3, right, one set of model parameters cannot be used to simultaneously simulate the first quarter tensile part and the hysteresis loops with high precision. Thus, the above model parameters can only be used as initial values for further optimization for the stabilized hysteresis loop.

6. Optimization of the model parameters

Two important factors, the kinematic hardening parameters and the initial yielding stress, have significant effects on the simulation. Based on the first quarter cycle, the initial yielding stress can be optimized with the CHK-3 model. It is well-known that the isotropic hardening rule will change the yield surface, which influences the shapes of the hysteresis loops. To identify the influence of the isotropic hardening on the model parameters, both the 150th cyclic test (the stabilized hysteresis loop) and the first cyclic test will be used for optimizing the CHK-3 model parameters, C_i, γ_i, and k.

6.1. *Optimization based on the first quarter tensile part.* The initial yielding stress definition, as pointed out by some authors [Facheris and Janssens 2014; Guijuan et al. 2014], has significant influence on the yield surface and the plastic flow directions. However, an exact definition for the yielding stress is not very clear at present. In [Abdel-Karim 2010], the author applied a smaller plastic strain offset (0.0025%) to determine the initial yielding stress. In the current work, the initial yielding stress (defined with a 0.02% plastic strain offset from the origin, where the initial yield stress is 232.251 MPa), serves as an initial value for optimization.

Because the CHK-3 model parameters will change with the alteration of the initial yielding stress, the following two steps are adopted in the optimization of the initial yielding stress:

(1) fixing C_i and γ_i to optimize k;

(2) fixing k to optimize C_i and γ_i.

Table 3 gives the optimal CHK-3 model parameters for the first quarter tensile curve. The optimized initial yielding stress is 181.392 MPa. Figure 7, left, shows the plastic stress strain response simulated by using the CHK-3 model with parameters before and after optimization. As a comparison, the first quarter tensile segment is also plotted in the figure.

Obviously, the simulated plastic stress-strain response produces a good agreement with the first tensile segment. In Figure 7, left, the calculated stress is always identical to zero when the plastic strain is substantially small and then it suddenly grows to the initial yielding stress k due to the large value of γ_1. This result proves that the aforementioned method is feasible.

6.2. *Optimization based on the first cyclic test.* In order to study the simulation capability of the initial values of the CHK-3 model parameters listed in Table 3 for the hysteresis loops, the cyclic plastic stress-strain response for the first cycle was calculated. Figure 7, right, shows the simulated plastic stress-strain response and the experimental test curve.

As illustrated in Figure 7, right, the shape of simulated plastic stress-strain response is remarkably different from the first cyclic test, especially at the transient portion. This can be attributed to the fact that the strain cycling leads to a decrease in the subsequent yielding stress when the first reverse occurs.

C_1	1444579.469	γ_1	21051.266
C_2	184230.879	γ_2	1749.424
C_3	22817.112	γ_3	278.154

**Table 3.** Optimum CHK-3 model parameters for the first quarter tensile curve.
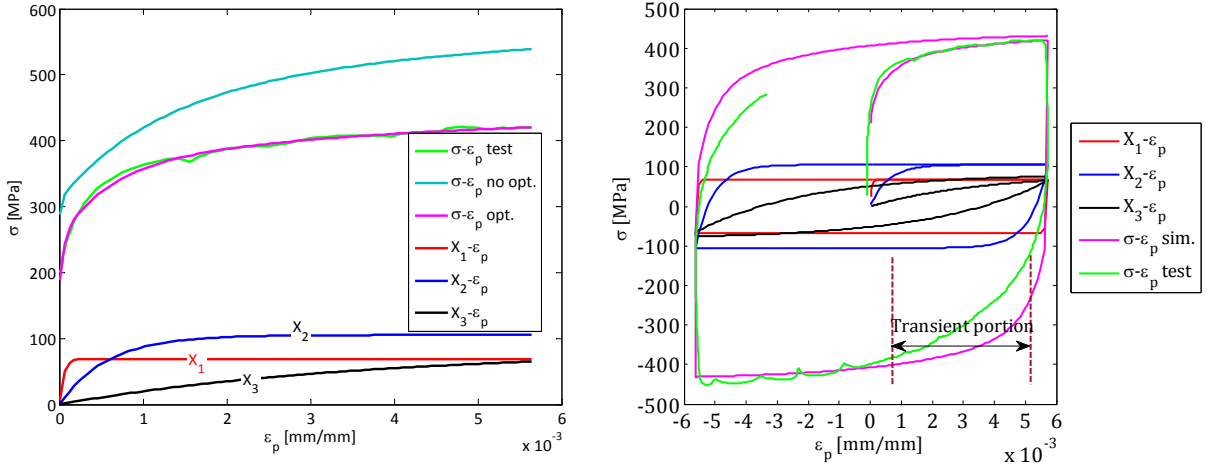
Figure 7. Left: comparison of the first quarter tensile part and the plastic stress-strain response simulated with and without parameter optimization. Right: comparison of the first cyclic test and the simulated plastic stress-strain response.

Because the values in Table 3 are determined from the uniaxial tensile part, there inevitably exists an overestimation when using them to simulate the first cycle.

To reduce the overestimation, another optimization was conducted based on the initial values for the first cycle. The plastic strain used in equations (5)–(7) was calculated based on the effective data shown in Figure 5, left, and the initial yielding stress is set to 181 MPa. Table 4 shows the optimal values of the CHK-3 model parameters for the first cyclic test. The simulated σ-ε_p response as well as the first cyclic test curve is plotted in Figure 8, left.

As seen in that graph, the simulation is in a good agreement with the first cyclic test except at the first quarter tensile segment. This suggests that the first quarter tensile curve and the cyclic test curves may not possess the same set of kinematic parameters if they exhibit a significant difference in shape.
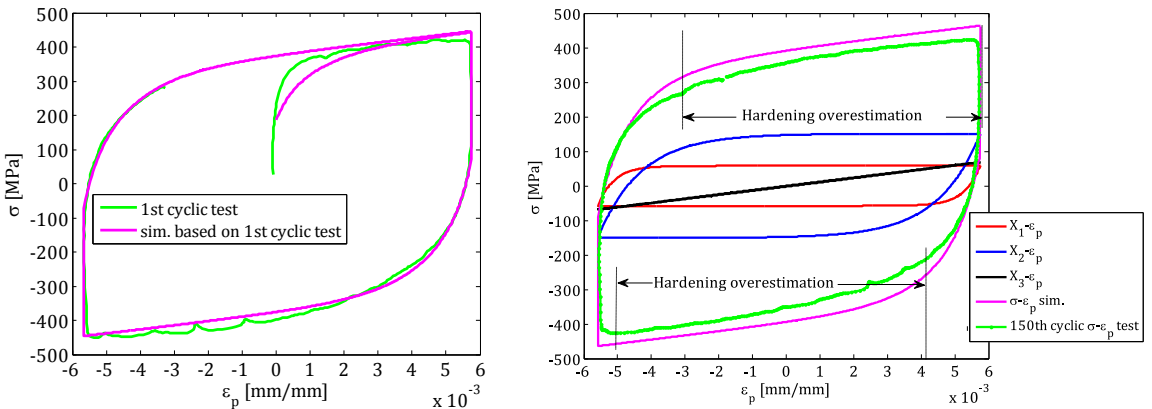
Figure 8. Left: comparison between the simulated σ-ε_p response and the first cyclic test. Right: comparison between the 150th cyclic test and σ-ε_p response simulated based on the parameters from Table 4.

The isotropic hardening could change the radius of the yield surface, causing the hysteresis loop to continuously change till it becomes the stabilized one. As a result, the kinematic hardening parameters will be different when respectively using the stable and unstable hysteresis loops to perform the parameter's optimization. To investigate these differences, a further optimization was executed with the stabilized hysteresis loop (the 150th cyclic test curve).

6.3. *Optimization based on the stabilized hysteresis loop.* The model parameters shown in Table 4 were used to simulate the stress-strain response for the stabilized hysteresis loop (the 150th cycle). Figure 8, right, gives the experimental σ-ε_p curve for the stabilized hysteresis loop and the σ-ε_p response simulated using the CHK-3 model with parameters listed in Table 4.

As shown in Figure 8, right, the simulated σ-ε_p curve exhibits a poor agreement with the 150th cyclic test. Qualitatively, the hardening overestimation in Figure 8, right, may be caused by the isotropic hardening. As analyzed in Section 6.2, the hysteresis loop continuously changes till it becomes a stabilized one due to the isotropic hardening effect. Consequently, the values of CHK-3 model parameters determined in Section 6.2 are not suitable for the stabilized hysteresis loop. Note that the cyclic softening occurs in the test. It is well-known, however, that 304SS should exhibit cyclic hardening under cyclic loading. The abnormal phenomenon may be ascribed to the high experimental frequency because an additional test at a frequency of 0.1 Hz exhibits the cyclic hardening effect; the additional test is displayed in Figure 9, left.

We thus draw the significant conclusion that the cyclic hardening behavior is rate-dependent. However, the method developed in this paper is feasible whatever the real material cyclic behavior.

C_1	122733.002	γ_1	3121.596
C_2	18641.186	γ_2	785.931
C_3	12127.629	γ_3	5.563

C_1	165362.400	γ_1	2372.604
C_2	80140.956	γ_2	834.633
C_3	18322.853	γ_3	0.111

Table 4. Optimal results of the CHK-3 model parameters for the first (left) and 150th (right) cyclic tests.
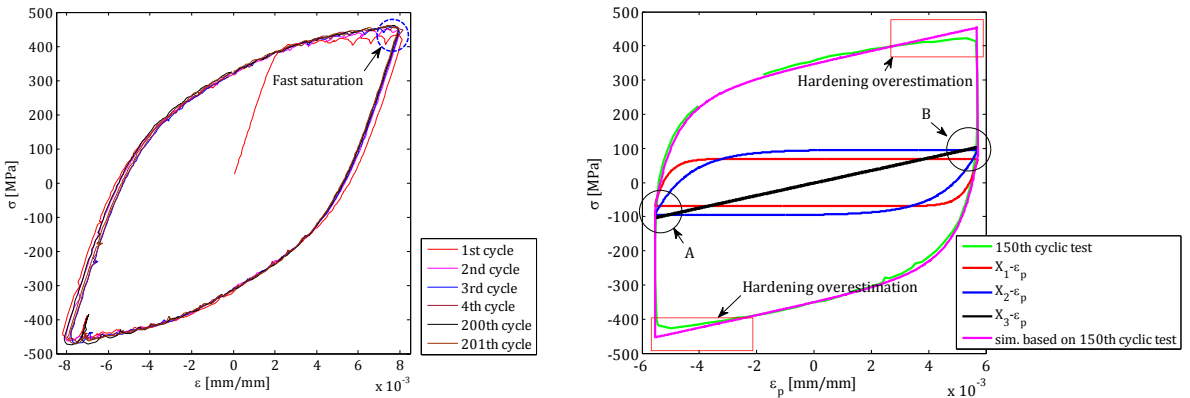
Figure 9. Left: stress-strain response at the strain-controlled test with test frequency of 0.1 Hz. Right: comparison between the 150th cyclic test and σ-ε_p response simulated based on the parameters from Table 4, right.

C_1	46318.993	γ_1	1501.795
C_2	80426.735	γ_2	1501.940
C_3	42612.671	γ_3	219.000

**Table 5.** CHK-3 model parameters optimized by fixing $\gamma_3 = 219$.

In the following optimization, the ratcheting parameter γ_3 was constrained to the range of 0.1 to 6 so as to meet the requirement for ratcheting simulation. Indeed, the reasonable value for γ_3 should be adjusted according to the ratcheting test, which has a slight effect on the hysteresis loop simulation. Table 4 also gives the optimized CHK-3 model parameters for the 150th experimental response.

Figure 9, right, shows the σ-ε_p response simulated with the CHK-3 model parameters from Table 4, right. For comparison, the 150th cyclic test curve is also plotted. We see that the simulation is in good agreement with experiments except at the regions near the peak of tension and the valley of compression. The fact is that the first and the second AF rule reach their saturated values before the relative plastic strain increases to a certain value, but the third AF rule does not. Thus, the hardening overestimation was closely associated with the third AF hardening rule.

The ratcheting parameter γ_3 has a significant effect on the ratcheting. As such, a reasonable value for γ_3 should be verified by the ratcheting test. In this investigation, we just want to verify the effect of γ_3 on the hysteresis loop. Accordingly, the reasonable ratcheting parameter for 304SS was not considered in a further optimization. Next, a special consideration for γ_3 was taken for obtaining a better simulation for the stabilized hysteresis loop.

As shown in Figure 9, right, hardening overestimation is ascribed to the fact that there exists a slow increasing/decreasing tendency in the third AF hardening rule. So, a larger value of γ_3 should be applied to increase its changing rate. To lower the effect of the third AF hardening rule on the hardening overestimation, a trial value of $\gamma_3 = 219$ was applied for an in-depth optimization.

The optimized values are given in Table 5. Figure 10 gives the σ-ε_p result calculated using the CHK-3
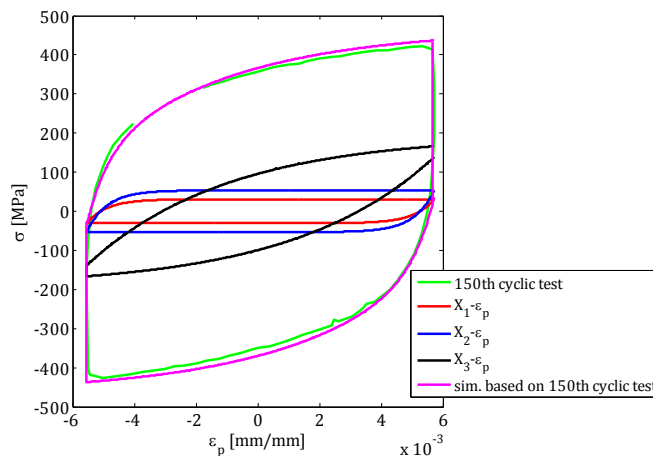
Figure 10. Comparison between the 150th cyclic test and σ-ε_p response simulated based on the parameters from Table 5.

model with the parameters given in Table 5. The 150th cyclic test is also plotted in the figure.

By comparing Figure 9, right, with Figure 10, we find that the simulation accuracy has been greatly improved by fixing the value of $\gamma_3 = 219$ to perform a new parameter optimization. As a consequence, the ratcheting parameter γ_3 actually has an effect on the hysteresis loop. Generally, however, a small change of γ_3 is enough to simulate the ratcheting evolution. Thus, the value of γ_3 for ratcheting is always assigned to a small value. The ratcheting parameter γ_3 in this work is not appropriate for ratcheting simulation, because a reasonable γ_3 should be verified through a further ratcheting test [Bari and Hassan 2000; Facheris and Janssens 2014]. Qualitatively, however, the parameters shown in Table 4, right, will be recommended for the ratcheting simulation, although they lead to a hardening overestimation.

7. Conclusions

The current work is devoted to identifying the CHK-3 model parameters with an algebraic calculation method based on its integral equations. The experimental test at strain range of $\pm 0.8\%$ was selected for optimizing the CHK-3 model parameters. The main conclusions for this paper are these:

(1) One same set of CHK-3 model parameters cannot ensure a same high precision when they are used simultaneously to simulate the stress-strain responses for both the first quarter tensile segment and the stabilized hysteresis loop.

(2) It is recommended removing the elastic loading/unloading segments from the experimental stress-strain curves before conducting an optimization of CHK-3 mode parameters.

(3) The initial yielding stress definition should be treated carefully for obtaining a good simulation. In this work, 232.251 MPa corresponding to 0.02% plastic strain offset was taken as the initial yielding stress, but after optimization, the reasonable initial yielding stress became around 181 MPa.

(4) The optimization procedure proposed can be applied generally to identify the CHK-3 model parameters for other similar metallic materials.

List of symbols

LCF	low cyclic fatigue
AF rule	Armstrong and Frederick kinematic hardening rule
LM algorithm	Levenberg–Marquardt algorithm
304SS	304 stainless steel
X_i	the i-th kinematic hardening rule
$C_i\ \gamma_i$	the ith Chaboche kinematic hardening parameters
E	Young's modulus
p	accumulated plastic strain
dp	accumulated plastic strain rate
$\underset{\approx}{\varepsilon}_{\mathrm{T}}$	total strain tensor
$\underset{\approx}{\dot{\varepsilon}}_{\mathrm{T}}$	total strain rate
$\underset{\approx}{\varepsilon}_{p}$	plastic strain tensor
$\underset{\approx}{\varepsilon}_{px}$	plastic x-axial strain

$\dot{\underset{\approx}{\varepsilon}}_p$	plastic strain rate
$\underset{\approx}{\varepsilon}_e$	elastic strain tensor
$\underset{\approx}{\varepsilon}_a$	strain amplitude
$\underset{\approx}{X}$	backstress tensor
$\underset{\approx}{S}$	deviatoric stress tensor
k	initial yielding stress
σ_x	x-axial stress
X_x	x-axial backstress
$\sigma_0\ \varepsilon_0\ n_0$	Ramberg–Osgood constants
σ_i^{sim}	the i-th simulated stress
σ_i^{exp}	the i-th experimental stress
ε_{th}	theoretical strain
ε_{fl}	fluctuating strain

Acknowledgments

References

[Abdel-Karim 2010] M. Abdel-Karim, "An evaluation for several kinematic hardening rules on prediction of multiaxial stress-controlled ratcheting", *Int. J. Plast.* **26**:5 (2010), 711–730.

[Ahmadzadeh and Varvani-Farahani 2013] G. Ahmadzadeh and A. Varvani-Farahani, "Ratcheting assessment of materials based on the modified Armstrong–Frederick hardening rule at various uniaxial stress levels", *Fatigue Fract. Eng. Mater. Struct.* **36** (2013), 1232–1245.

[Armstrong and Frederick 1966] P. Armstrong and C. Frederick, "A mathematical representation of the multiaxial Bauscinger effect", CEGB Report RD/B/N731, 1966. Reproduced in *Materials at High Temperatures* **24**:1 (2007), 11–26.

[ASTM E606/E606M 2012] "Standard test method for strain-controlled fatigue testing", ASTM Standard E606/E606M, ASTM International, 2012.

[Bari and Hassan 2000] S. Bari and T. Hassan, "Anatomy of coupled constitutive models for ratcheting simulation", *Int. J. Plast.* **16** (2000), 381–409.

[Benham 1965] P. Benham, "Some observations on the cyclic strain-induced creep in mild steel at room temperature", *Int. J. Mech. Sci.* **7**:2 (1965), 81–86.

[Besson et al. 1998] J. Besson, R. Leriche, R. Foerch, and G. Cailletaud, "Object-oriented programming applied to the finite element method, II: Application to material behaviors", *Rev. Européenne Élém. Finis* **7**:5 (1998), 567–588.

[Chaboche 1986] J. Chaboche, "Time-independent constitutive theories for cyclic plasticity", *Int. J. Plast.* **2**:2 (1986), 149–188.

[Chaboche 1988] J. Chaboche, "Continuum damage mechanics, I: General concepts", *J. Appl. Mech.* (*ASME*) **55**:1 (1988), 55–64.

[Chaboche 1991] J. Chaboche, "On some modifications of kinematic hardening to improve the description of ratcheting effects", *Int. J. Plast.* **7**:7 (1991), 661–678.

[Chaboche 2008] J. Chaboche, "A review of some plasticity and viscoplasticity constitutive theories", *Int. J. Plast.* **24**:10 (2008), 1642–1693.

[Chaboche et al. 1979] J. Chaboche, K. Dang Van, and G. Cordier, "Modelization of the strain memory effect on the cyclic hardening of 316 stainless steel", art. id. L11/3 in *Transactions the 5th International Conference on Structural Mechanics in Reactor Technology* (Berlin, 1979), North-Holland, Amsterdam, 1979.

[Chaboche et al. 2012] J. Chaboche, P. Kanouté, and F. Azzouz, "Cyclic inelastic constitutive equations and their impact on the fatigue life predictions", *Int. J. Plast.* **35** (2012), 44–66.

[Dafalias et al. 2008] Y. Dafalias, K. Kourousis, and G. Saridis, "Multiplicative AF kinematic hardening in plasticity", *Int. J. Solids Struct.* **45**:10 (2008), 2861–2880.

[Djimli et al. 2010] L. Djimli, L. Taleb, and S. Meziani, "The role of the experimental data base used to identify material parameters in predicting the cyclic plastic response of an austenitic steel", *Int. J. Press. Vessels Pip.* **87**:4 (2010), 177–186.

[Egner and Egner 2014] H. Egner and W. Egner, "Modeling of a tempered martensitic hot work tool steel behavior in the presence of thermo-viscoplastic coupling", *Int. J. Plast.* **57** (2014), 77–91.

[Facheris and Janssens 2014] G. Facheris and K. Janssens, "An internal variable dependent constitutive cyclic plastic material description including ratcheting calibrated for AISI 316L", *Comput. Mater. Sci.* **87** (2014), 160–171.

[Guijuan et al. 2014] H. Guijuan, Z. Keshi, and M. Zhili, "Numerical analysis on subsequent yield surfaces and plastic flow direction of 45 steel by Chaboche model", *J. Guangxi Univ. Nat. Sci. Ed.* **39** (2014), 171–179. In Chinese.

[Jiang et al. 2009] Y. Jiang, W. Ott, C. Baum, M. Vormwald, and H. Nowack, "Fatigue life predictions by integrating EVICD fatigue damage model and an advanced cyclic plasticity theory", *Int. J. Plast.* **25**:5 (2009), 780–801.

[Jiang et al. 2013] X. Jiang, Y. Zhu, J. Hong, Y. Zhang, and Q. Kan, "Constitutive model for time-dependent ratcheting of SS304 stainless steel: simulation and its finite element analysis", *J. Méc. Théor. Appl.* **51**:1 (2013), 63–73.

[Kamaya and Kawakubo 2015] M. Kamaya and M. Kawakubo, "Loading sequence effect on fatigue life of type 316 stainless steel", *Int. J. Fatigue* **81** (2015), 10–20.

[Li et al. 2014] J. Li, C. Li, Y. Qiao, and Z. Zhang, "Fatigue life prediction for some metallic materials under constant amplitude multiaxial loading", *Int. J. Fatigue* **68** (2014), 10–23.

[Ohno and Wang 1994] N. Ohno and J. Wang, "Kinematic hardening rules for simulation of ratchetting behavior", *Eur. J. Mech. A Solids* **13**:4 (1994), 519–531.

[Pereira and Jesus 2011] H. Pereira and A. Jesus, "Fatigue modeling of a notched geometry under spectrum block loading supported on elastoplastic FEA", *Procedia Eng.* **10** (2011), 1354–1359.

[Prager 1956] W. Prager, "A new method of analyzing stresses and strains in work hardening plastic solids", *J. Appl. Mech. (ASME)* **23** (1956), 493–496.

[Rahman 2006] S. Rahman, *Finite element analysis and related numerical schemes for ratcheting simulation*, Ph.D. thesis, North California State University, 2006, available at http://www.lib.ncsu.edu/resolver/1840.16/5967.

[Taleb and Cailletaud 2010] L. Taleb and G. Cailletaud, "An updated version of the multimechanism model for cyclic plasticity", *Int. J. Plast.* **26**:6 (2010), 859–874.

[Velay et al. 2006] V. Velay, G. Bernhart, and L. Penazzi, "Cyclic behavior modeling of a tempered martensitic hot work tool steel", *Int. J. Plast.* **22**:3 (2006), 459–496.

[Voyiadjis and Basuroychowdhury 1998] G. Voyiadjis and I. Basuroychowdhury, "A plasticity model for multiaxial cyclic loading and ratcheting", *Acta Mech.* **126**:1 (1998), 19–35.

LIU SHIJIE: shi.jieliu@163.com
School of Astronautics, Beihang University (Beijing University of Aeronautics and Astronautics),
Xueyuan Road 37#, Haidian district, Beijing, Beijing, 100191, China

LIANG GUOZHU: lgz@buaa.edu.cn
School of Astronautics, Beihang University (Beijing University of Aeronautics and Astronautics),
Xueyuan Road 37#, Haidian district, Beijing, Beijing, 100191, China

JOURNAL OF MECHANICS OF MATERIALS AND STRUCTURES

msp.org/jomms

Founded by Charles R. Steele and Marie-Louise Steele

Cover photo: Mando Gomez, www.mandolux.com

Journal of Mechanics of Materials and Structures

Volume 12, No. 4   July 2017